Evaluation of a New Airborne Microwave Remote Sensing Radiometer by Measuring the Salinity Gradients Across the Shelf of the Great Barrier Reef Lagoon

Yonghong Wang, Malcolm L. Heron, *Senior Member, IEEE*, Arnstein Prytz, Peter V. Ridd, Craig R. Steinberg, and Jörg M. Hacker

***Abstract*—Over the last ten years, some operational airborne remote sensing systems have become available for mapping surface salinity over large areas in near real time. A new dual-polarized Polarimetric L-band Multibeam Radiometer (PLMR) has been developed to improve accuracy and precision when compared with previous instrument generations. This paper reports on the first field evaluation of the performance of the PLMR by measuring salinity gradients in the central Great Barrier Reef. Before calibration, the raw salinity values of the PLMR and conductivity–temperature–depth (CTD) differed by 3–6 psu. The calibration, which uses *in situ* salinity data to remove long-term drifts in the PLMR as well as environmental effects such as surface roughness and radiation from the sky and atmosphere, was carried out by equating the means of the PLMR and CTD salinity data over a subsection of the transect, after which 85% of the salinity values between the PLMR and CTD are within 0.1 psu along the complete transect. From offshore to inshore across the shelf, the PLMR shows an average cross-shelf salinity increase of about 0.4 psu and a decrease of 2 psu over the inshore 20 km at -19° S (around Townsville) and -18° S (around Lucinda), respectively. The average cross-shelf salinity increase was 0.3 psu for the offshore 100 km over all transects. These results are consistent with the *in situ* CTD results. This survey shows that PLMR provided an effective method of rapidly measuring the surface salinity in near real time when a calibration could be made.**

***Index Terms*—Great Barrier Reef (GBR), microwave radiometer, remote sensing, sea surface salinity.**

I. Introduction

HIGH-PRECISION multibeam airborne microwave radiometers are the leading technology for the remote sensing of sea surface salinity. Although microwave L-band radiometers and aircraft had been combined in an attempt to measure sea surface salinity by the early 1970s, long delays were experienced in developing practical systems due to the technical difficulties of measuring very low radiation intensities. Since the early 1990s, a number of airborne microwave radiometers have been designed, built, and tested. Examples include the Electronically Scanning Thinned Array Radiometer [9], the Passive/Active L/S-band Airborne Sensor [19], [20], the Scanning Low-Frequency Microwave Radiometer (SLFMR) [5], and the Salinity, Temperature, and Roughness Remote Scanner (STARRS) [4], [12]. In 2000, an instrument that is based on the prototype SLFMR [5], [11], [13] was constructed for an Australian research consortium by Quadrant Engineering (now ProSensing), Amherst, MA. The SLFMR instrument has been used in the study of the estuarine plume of the Herbert River in the Great Barrier Reef (GBR), and results on the structure and influence of tropical river plumes were obtained [3].

For the Australian SLFMR, the absolute accuracy of the instrument was empirically determined by using *in situ* observations with a conductivity–temperature–depth (CTD) probe, and it was found that the calibration with respect to ground-truth data drifted over a salinity range of 3 psu [3]. To improve the precision, a new-generation microwave radiometer was developed in 2004 based on the SLFMR and the STARRS radiometer technology. This new-generation instrument, namely the dual-polarized Polarimetric L-band Multibeam Radiometer (PLMR), was built for the Australian group by ProSensing and delivered in March 2005.

The designs of the SLFMR and PLMR are based on the work of Blume *et al.* [2] and Ulaby *et al.* [16]. While the SLFMR uses a Dicke switch that is balanced by a feedback loop, the PLMR uses three reference noise sources that are referred to as cold (130 K), warm (310 K), and hot (600 K) calibration loads, which is an extension of the design with two reference loads [7]. By sequentially sampling the receiver output through a cycle of four switch positions to the antenna and calibration loads, the PLMR can eliminate the noise power that is introduced by the receiver parameters, namely gain, bandwidth, noise

Manuscript received August 12, 2006; revised April 29, 2007. This work was supported in part by the Australian Research Council under Discovery Grant DP0558516 (for the study on the flushing time of the GBR lagoon), by the Office of Naval Research under Global Award N00014-04-1-0700 (for the development of remote sensing of salinity at James Cook University), and by the National Natural Science Foundation of China under Grant 40406015.

Y. Wang is with the College of Marine Geoscience, Ocean University of China, Qingdao 266100, China, and also with the Marine Geophysical Laboratory, James Cook University, Townsville, Qld. 4811, Australia (e-mail: yonghong.wang@jcu.edu.au; yonghongw@ouc.edu.cn).

M. L. Heron and P. V. Ridd are with the AIMS@JCU and Marine Geophysical Laboratory, James Cook University, Townsville, Qld. 4811, Australia (e-mail: qsec@austarnet.com.au; peter.ridd@jcu.edu.au).

A. Prytz is with the Marine Geophysical Laboratory, James Cook University, Townsville, Qld. 4811, Australia (e-mail: arnstein.prytz@jcu.edu.au).

C. R. Steinberg is with the AIMS@JCU and Australian Institute of Marine Science, Townsville, Qld. 4810, Australia (e-mail: C.Steinberg@aims.gov.au).

J. M. Hacker is with the Airborne Research Australia, Flinders University, Salisbury South, S.A. 5106, Australia (e-mail: jorg.hacker@flinders.edu.au).

Digital Object Identifier 10.1109/TGRS.2007.903400

temperature, and antenna loss. The two radiometers differ in the manner in which the beams are formed and sampled. In the SLFMR, the radiometer operates in a vertically polarized mode at 1.413 GHz with a bandwidth of 24 MHz and uses 64 dipole antennas that are set out in an array of 8×8 dipoles. The beams are formed entirely in hardware using a passive Butler matrix to form eight beams, which are scanned sequentially in the across-track plane to form a swath parallel to the aircraft track at nominal incidence angles of $\pm 8^\circ$, $\pm 22^\circ$, $\pm 37^\circ$, and $\pm 61^\circ$ away from the nadir [15].

The PLMR has some other important differences from the SLFMR. These are as follows: 1) the PLMR utilizes vertical and horizontal polarizations; 2) the PLMR has six separate receiver channels, which are sampled simultaneously; and 3) the PLMR observes the sea surface salinity by a fixed push-broom swath rather than a scanning pattern. In the scanning pattern of SLFMR, the radiometer samples for 0.5 s and internal overheads during beam switching add 0.135 s. Thus, a swath of six beams (deliberately excluding the two outer beams) is completed in 3.810 s, and the beam pattern is staggered with respect to the aircraft across-track direction. In the push-broom swath of PLMR, where there is no need to switch beams, each swath is completed in 0.660 s, including a 0.135-s overhead. In this time, both polarizations for all six beams are sampled. For the SLFMR, the aircraft moves 250 m before it samples the next spot, and we can have 4 samples in a 1-km distance. In addition, in all previous applications, the SLFMR has been used for swath mapping. In this application, we are interested in a 1-D transect, and we assume that each beam gives an independent sample along the transect (ignoring the second dimension). This gives a sixfold increase in sampling. Each beam in the PLMR, with the same altitude and a slower speed of 40 m/s, can sample 25 times in the time it takes for the aircraft to fly 1 km. Thus, for the six beams in 1 km, we have 300 samples of sea surface salinity in the two polarizations. With this pattern using the PLMR, we have a factor of 276 more salinity samples than with the SLFMR. This significantly improves the performance by reducing the noise.

PLMR is one of the leading technologies for the remote sensing of the sea surface using aircraft, but the challenge in this deployment is to determine the instrument accuracy and precision. One of the critical issues when using this technique is deciding on the algorithms that convert radiometer output to determine the observed brightness temperature and then the seawater conductivity when internal temperatures of the radiometer housing are varying. Although there has been a substantial literature on L-band microwave radiometer design and development, practical demonstrations of these instruments on large-scale surveys are still rare. This paper is the first to describe the field performance of the PLMR and dual-polarized radiometer. We focus on the description of the overall operational performance and calibration of the PLMR in mapping salinity gradients in the GBR lagoon.

The field area for testing the PLMR performance was the central section of the GBR lagoon (see Fig. 1), where a study was being conducted to determine the flushing time of the lagoon by using water salinity as a passive tracer. This study of the GBR flushing time was a convenient project in which to test

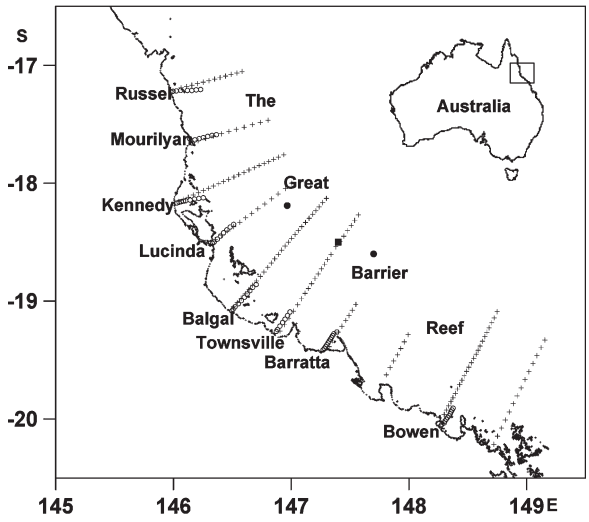

Fig. 1. Location of the field area (the central GBR lagoon) and the transect distribution. The "+" and "○" represent the locations of the salinity transects obtained from the PLMR and CTD on July 11–16, 2005, respectively. "■" is the offshore position that the CTD data were collected on November 29, 2005, and "●" represents the position that the CTD data were collected on April 17 and September 1, 2005 (details in Table I).

the PLMR, as *in situ* observations of water salinity were also being made using a boat with a CTD profiler. In addition, unlike previous studies in the GBR lagoon using the SLFMR, this paper was done in the dry season, where river flow was either zero or very small southward from Townsville and no significant river plumes were present. Instead, a coastally attached band of water about 15 km wide exhibited hypersaline conditions of up to 0.75 psu for much of the region. This hypersalinity was due to evaporation. It is not possible to assume zero freshwater discharge north of Townsville even in the dry season. However, if there are no large unseasonable rain events and consequent transient river plumes, a moderate reduction in salinity of a few practical salinity units at the coast is to be expected. The small and gently varying salinity gradients in the study area were ideally suited for testing the stability, accuracy, and precision of the PLMR.

II. Methods

A. Specifications of PLMR and Ground Test

1) Specifications of PLMR: Components of the PLMR, which must be placed outside the aircraft under the fuselage, are housed in a thermally controlled and aerodynamically shaped enclosure measuring 0.38 m high $\times$ 1.04 m wide $\times$ 1.04 m long and with a mass of 47.6 kg. There are five thermometers, which are distributed in the middle, and four corners of the enclosure, which measure the temperature of the antenna array. Other system components, including a power supply, a computer that is used to control and acquire data from the antenna, and a GPS receiver, are mounted on an equipment rack inside the airplane, measuring 0.56 m high $\times$ 0.58 m wide $\times$ 0.58 m long and weighing 18.6 kg. Both the enclosure and the rack for the PLMR are lighter than those for the SLFMR. This means that the PLMR assembly can be fitted to a Small Environmental Research Aircraft, which, in this case, is a Diamond Aircraft

HK36TTC-ECO Dimona aircraft, which is a motorized glider. By using this smaller aircraft, it is possible to reduce operational cost. The glider has a lower stall speed so that it can cruise at a slower speed (30–50 m/s) and more data can be collected along the track, thus improving the accuracy.

The PLMR spatial resolution (beam spot size) is approximately 0.3 times the altitude, and the swath width is about twice the altitude. The PLMR can operate from a 240-Vac, 49- to 61-Hz electrical power, drawing a maximum of about 1 A from the aircraft supply. The power/communications module in the aircraft converts the 240-Vac input power to +28 Vdc, which is then distributed to the PLMR electronics.

There are two underwing pods in the aircraft, and each pod can support a maximum instrument load of 55 kg. An infrared radiometer and other sensors were installed in one of the underwing pods. In addition, the light aircraft carries other standard instrumentations for remote sensing, including the FLIRTS SC60 infrared imager with a 0.08-K resolution, which was mounted in an underwing pod, a three-charge-coupled device digital video camera, a trispectral line scanner, a radar altimeter with 0.1-m resolution and 1.5-m accuracy, and a GPS-based attitude system (Trimble TANS Vector 10 Hz, 0.1° accuracy) for pitch and roll angles and aircraft heading. The endurance of the aircraft is 4–8 h with a range of about 800–1500 km.

2) PLMR Ground Tests: Calibrations were carried out to evaluate the stability of the PLMR system. We call these ground test calibrations to separate the calibrations that were done later with *in situ* CTD probes. Ground test calibration procedures are used before and after every salinity mapping flight. During the ground test calibrations, we use the "cold sky" as one target and assume it to be 5.5 K following [10]. Care must be taken to ensure that the PLMR does not point at a section of the sky that is occupied by the sun, the moon, or the galaxy. A specially constructed calibration chamber that was lined with microwave absorber cones was used as a second stable target at ambient air temperature with a microwave brightness temperature around 279 K. The temperature of the chamber was monitored using internally mounted temperature sensors. During the ground test calibrations, the PLMR was first pointed to the sky and then pointed into the chamber to test the stability of the PLMR and provide calibration data for the instrument.

A sequence of initial calibration checks was carried out on the PLMR. On February 14 and 15, 2005, the manufacturer performed a calibration test with the chamber for 6.7 h and a sky test of 6.4 h. From March 15 to 18, 2005, the PLMR was tested in Adelaide, Australia, with a chamber calibration lasting 21 h and the sky calibration lasting 8 h. During the fieldwork on the GBR lagoon, from July 11 to 16, 2005, 15-min ground test calibrations (both sky and chamber tests) were completed before and after each daily flight.

B. Salinity Data Acquisition

1) PLMR Salinity Data Acquisition: In the morning of July 11, 2005, the PLMR and all its components were installed on the aircraft. Because the brightness temperature is affected by sun glint, most flights were scheduled in the early morning to reduce the influence of sun glint. During the mapping process from July 11 to 16, 2005, flight altitudes were about 3.6–4.3 km, and ground speeds averaged about 40 m/s. Before the aircraft entered the research transects, it flew for about 0.5–1 h to allow the PLMR temperature to stabilize at altitude. For each flight, the aircraft flew two transects (about 100 km). The flight times and transects are listed in Table I and shown in Fig. 1.

2) CTD Salinity Data Acquisition: Simultaneously with the PLMR flights from July 11 to 16, 2005, we carried out *in situ* salinity measurements using a Sea Bird SBE 19 CTD probe 20–30 km along the transect from a 5-m boat. The procedure involved stopping the boat at selected GPS coordinates about every 1–2 km and taking a vertical CTD profile. Weather conditions determined how far offshore the *in situ* transect could be taken from the small boat. We also measured the CTD salinity along a transect for about 100 km from Townsville using a chartered fishing boat on November 29, 2005. In addition, the salinity in the offshore 80–120 km near Townsville and Lucinda transects was measured by an Australia Institute of Marine Science research vessel on April 17 and September 1. Positions at which salinity was measured are shown in Fig. 1. Table I provides a detailed summary of the coordinates and times of the various transects.

C. Instrument Calibration

1) Correction of Brightness Temperature Calibration Coefficients: One of the features of the PLMR design is the management of the effect of variations in the internal temperature of the instrument on the brightness temperature data. The instrument housing is maintained at a constant temperature (usually set at about 40 °C) by five internal heater banks that are mounted on the structural ground plane for the antenna patches, each heater bank with a separate temperature sensor in a feedback control loop. This is a coarse control and does not deal with temperature gradients within the instrument housing. The effect of these gradients and also any "hunting" in the feedback control loop are removed by calibration. A series of temperature sensors is placed at key positions within the instrument, and a set of calibration coefficients is determined during a calibration procedure. To do this, we assume that the correction to brightness temperature due to fluctuations at each sensor by using the laboratory and field data is linear and that the corrections due to all of the sensors can be superposed according to the manufacturer's calibration (1), where the scene brightness temperature T_{Bn} for antenna beam n can be calculated using

$$T_{Bn} = a_{0n} + a_{1n} \times \frac{t_F}{35} + a_{2n} \times \frac{t_{Rn}}{35} + a_{3n} \times \gamma_n + a_{4n} \times \gamma_n \times \frac{t_{Rn}}{35} \quad (1)$$

where a_{in} ($i = 0{-}4$ and $n = 1{-}6$) are the T_B calibration coefficients, and a unique set of five coefficients exists for each of the 12 PLMR beam and polarization combinations. The variable t_F represents the average antenna temperature as calculated from the mean of the five internal temperature sensors at the center and four corners of the antenna back plane,

TABLE I
BOAT AND AIRCRAFT TRANSECT SUMMARY

Transect Location	Data Type	Start-finish time	Start-finish lat(S)	Start-finish long(E)	Distance /km	Processing time (h)*	Flight altitude km	Ground speed m/s
Bowen	PLMR	11 July 15:38-16:44	19.0615 19.9782	148.7693 148.2913	113.5	1.1	4.3	30-50
	CTD	11 July 09:09-11:32	20.064 19.899	148.2684 148.3782	21.6	2.4		
Barratta	PLMR	12 July 8:03-08:25	19.0204 19.3983	147.5617 147.3158	49.3	0.4	4.3	35-45
	CTD	12 July 10:54-12:23	19.4158 19.2614	147.2689 147.3884	21.2	1.5		
Townsville	PLMR	14 July 06:33-07:35	19.2978 18.2607	146.8759 147.5753	136.7	1.0	4.3	30
	CTD	14 July 07:56-09:29	19.2759 19.0618	146.8631 147.0103	28.4	1.5		
Balgal	PLMR	14 July 07:48-09:04	18.0967 19.0777	147.3315 146.4882	140.6	1.3	4.3	30
	CTD	14 July 10:54-12:40	18.8705 19.0894	146.6866 146.4892	31.9	1.7		
Lucinda	PLMR	15 July 06:46-07:25	18.5156 17.9521	146.3119 147.0615	100.9	0.7	3.6	30-45
	CTD	15 July 8:56-9:39	18.5156 18.3491	146.3227 146.5118	27.2	0.7		
Kennedy	PLMR	15 July 07:35-08:34	17.7579 18.1658	146.9408 146.0212	107.3	1.0	3.6	30-40
	CTD	15 July 11:09-13:05	18.1218 18.1749	146.2727 146.0128	28.1	2.0		
Mourilyan	PLMR	16 July 07:09-07:36	17.6596 17.4606	146.1493 146.8117	73.6	0.4	3.6	30-40
	CTD	16 July 7:14-8:55	17.6223 17.5868	146.1373 146.384	36.4	0.9		
Russel	PLMR	16 July 07:54-08:32	17.0421 17.2113	146.6349 145.9763	72.4	0.6	3.6	30-40
	CTD	16 July 11:11-13:15	17.2054 17.2246	146.2308 145.9492	29.9	2		
Offshore (●)	CTD	17 April 1 September	18.1896	146.9664				
	CTD	17 April 1 September	18.5619	147.952				
Offshore (■)	CTD	29 November	18.5121	147.4023				

*The Processing time refers to the time that the aircraft flew to obtain the data over a certain distance.

i.e., $t_F = (t_1 + t_2 + t_3 + t_4 + t_5)/5$, where t_5 is the middle antenna temperature, and t_1 to t_4 are the four corner temperatures. t_{Rn} are the six receiver temperatures. γ_n corresponds to the output signal from the receivers.

The T_B calibration coefficients a_{in} are determined by a multivariate least squares linear regression procedure. This involves pointing the PLMR at a known target temperature and varying the internal temperatures t_f and t_{Rn}. T_B is known from the target temperature, and γ_n is the output of the PLMR. We choose target temperatures at extremes that encompass the range of seawater brightness temperatures of around 100 K (at 1.4 GHz).

Fig. 2(a) shows the calibration chamber T_B for each of the six beams during the 15-min ground test before the flight on July 11, 2005, using the manufacturer's calibration coefficients. Ideally, T_B should be the same for each beam. However, it is evident from Fig. 2(a) that there is up to a 2-K difference between beams, and this indicates some drift in the calibration in the intervening time. The temperature change of the target of about 1.5 K during the calibration is a local heating effect, which is not relevant to the differences between the beams. Clearly, to obtain a consistent behavior for all beams, new calibration coefficients are needed.

The PLMR is calibrated against the sky and the calibration chamber before and after each flight. This allows the ability to take account of changes in the calibration of the instrument within and between flights. Without these corrections, errors can be on the order of a few kelvins.

The aircraft flies at an altitude of around 4000 m along the transects; the cabin is not pressurized, and the pilot uses comfortable nasal cannulas that are connected to an on-demand oxygen system. Fig. 3 shows that the antenna temperatures

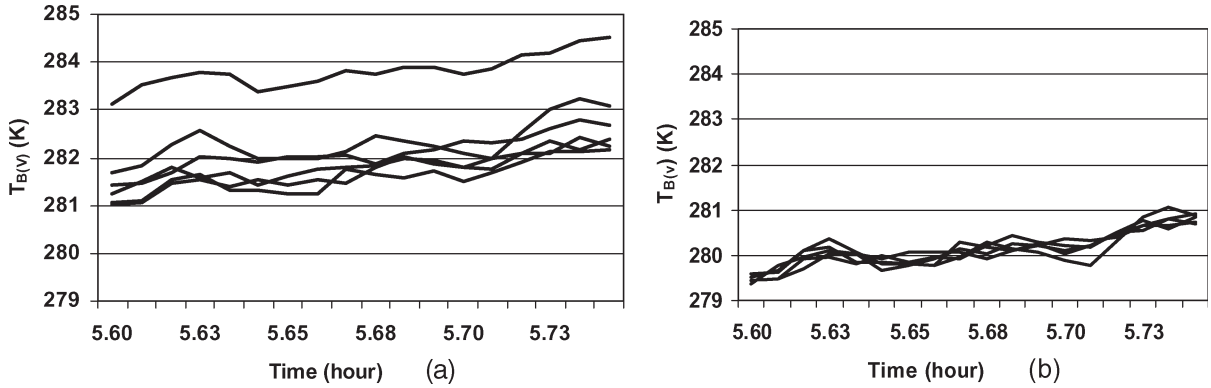

Fig. 2. Six T_B values for the vertical polarization during the ground chamber test on July 11, 2005. The temperature of the target changes because of heating from the PLMR. These results show comparisons between the beams. (a) T_B values using the manufacturer's calibration coefficients. (b) T_B values using new calibration coefficients.

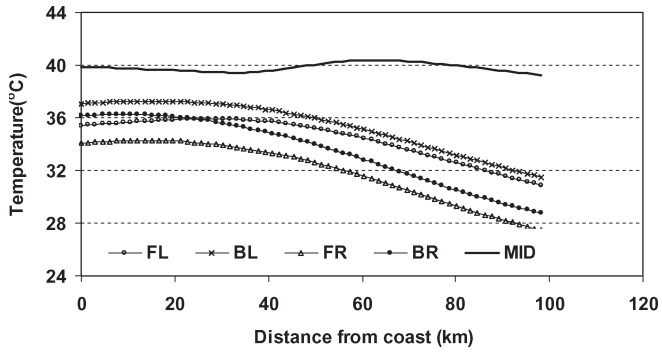

Fig. 3. Five internal antenna temperatures during the Lucinda transect. The abscissa represents the distance along the transect. FL, FR, BL, BR, and MID represent the front left, front right, back left, back right, and middle temperature sensors in the PLMR, respectively.

change with distance along the Lucinda transect, not because of changes in the external atmospheric temperature but because of a temporal response of the thermal system at that altitude. Ideally, these five antenna temperatures would be the same and not vary with time if the internal heating mechanisms of the PLMR were working effectively. It was found that the middle and four corner antenna temperatures did not respond in the same way to changes in ambient temperature. It is also evident from Fig. 3 that there is a temporal variation in the temperature of up to 5 °C, particularly after the first 30 km of the transect. The high temperature gradient within the instrument implies that there is a considerable heat loss through the sides of the instrument. These phenomena were found to be repeated in the other transects.

To compensate for internal temperature gradients, a more elaborate calibration scheme was adopted. Equation (1) uses only the average of the internal antenna temperature measurement. Inspection of Fig. 3 shows that the middle antenna temperature is different from the corner temperatures and that the corner temperatures behave similarly to each other. The modified calibration scheme takes this into account the following:

$$T_{Bn} = b_{0n} + b_{1n}\frac{t_{\mathrm{mid}}}{35} + b_{2n}\frac{t_{Rn}}{35} + b_{3n} \times \gamma_n + b_{4n} \times \gamma_n \times \frac{t_{Rn}}{35} + b_{5n}\frac{t_{\mathrm{corner}}}{35} \quad (2)$$

where t_F in (1) has been separated into two terms: t_{mid} and t_{corner}. t_{mid} is the middle antenna temperature (t_5), and $t_{\mathrm{corner}} = (t_1 + t_2 + t_3 + t_4)/4$. b_{in} $(i = 0{-}5$ and $n = 1{-}6)$ corresponds to the modified calibration coefficients. These modified calibration coefficients are calculated in a similar manner to the a_{in} values.

Fig. 2(b) shows that the use of (2) considerably reduced the PLMR beam-to-beam differences with variations reduced by an order of magnitude.

2) Obtaining Salinity From the Brightness Temperature: The PLMR responds to the target brightness temperature that is associated with changes in the microwave emissivity and the physical temperature of the sea surface. The microwave emissivity, to first order, is a function of both the physical temperature and salinity of the surface. Using the algorithm of Klein and Swift [8], the brightness temperature of the water as measured by the PLMR can be converted to salinity. This model requires the sea surface temperature that in this case was remotely sensed using an Everest infrared radiometer that was mounted in an instrument rack in an underwing pod on the aircraft. The infrared radiometer was calibrated in laboratory conditions by independently varying the target temperature and the radiometer body temperature.

The conversion of brightness temperature is sensitive to several corrections due to the physical effects that alter the brightness temperature independently from the salinity signal. These effects include sea roughness, which is normally introduced as a wind-dependent correction, sky radiation that is reflected from the sea surface up into the radiometer, and atmospheric radiation both downwelling and reflected back into the radiometer, and upwelling radiation from the air beneath the aircraft. In our experiment, there is also an atmospheric effect of radiation in the infrared band, which will increase the measured infrared temperature.

The most significant correction is that for surface roughness. The European Space Agency-sponsored Wind and Salinity Experiment [1] used a radiometer that was mounted on the Casablanca oil platform and supporting measurements to evaluate the effect of wind speed on the brightness temperature of the sea surface emission. They found a linear relationship of 0.25 $\mathrm{K}/(\mathrm{m} \cdot \mathrm{s})$ for a downward-looking radiometer. In our experiments, we chose days with light winds to be able to

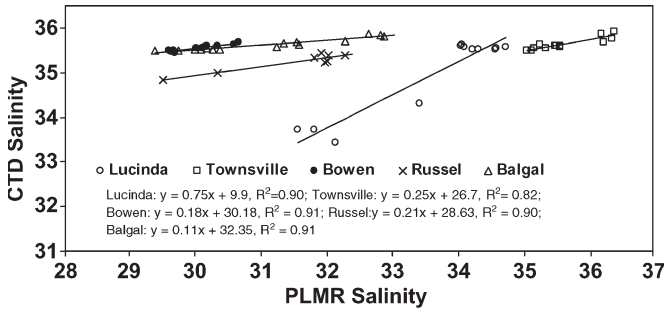

Fig. 4. Regression relationship of PLMR sea surface salinity versus CTD salinity of inshore 30–40 km of five transects. Data points represent the average of all six beams and both polarizations over 1 km for the PLMR data.

operate the open dinghy for the CTD *in situ* measurements. Furthermore, all of the environmental corrections are manifested on a large scale, and we have assumed that they are constant along each transect. Thus, when we adjust the offset in salinity between the PLMR data and the CTD data, we are removing all of these environmental effects (as well as the long-term drift effects in the PLMR). Effectively, we are assuming that any variations in the environmental corrections are less than the variations in salinity. The choice of low-wind days helps the credibility of this assumption, and the agreement between the adjusted PLMR salinity and the offshore CTD data vindicates the assumption.

3) Correction Using CTD Data: The salinity data derived from the PLMR measurements can be further improved if some CTD measurements are taken at times and positions coincident with the PLMR. The PLMR data were processed by smoothing the data from each beam in the along-track direction using a moving average boxcar filter having a window length of 0.5 km. The CTD cast data were also smoothed with a 1- to 3-m-long boxcar filter, depending on the cast depth. Regressions were performed between the PLMR and CTD data to apply a final correction to the PLMR data, and each transect has its own regression, which is shown in Fig. 4. The inshore CTD data (Table I) were used to derive the regression equations, and they were tested on the single-point CTD measurements taken further offshore to determine the error in the final calibrated salinity measurements. The offshore CTD measurements were not used to develop the regression equations.

III. Results

A. PLMR Accuracy

Fig. 4 shows a comparison of PLMR salinity data before CTD correction using data measured by the CTD profiler for the inshore 30 km of various transects. The regression equations differ significantly from the ideal, where we expect a slope of 1 and an intercept of 0. For different transects, slope varies greatly between 0.11 and 0.75. Despite the large divergence between the raw PLMR and CTD data, a high correlation exists at most sites between the two data sets $(R^2 = 0.82{-}0.91)$, and thus, an empirical correction can be made to improve the accuracy of the PLMR data. An R^2 correlation of less than 0.5 exists for the Baratta, Mourilyan, and Kennedy transects due to significant

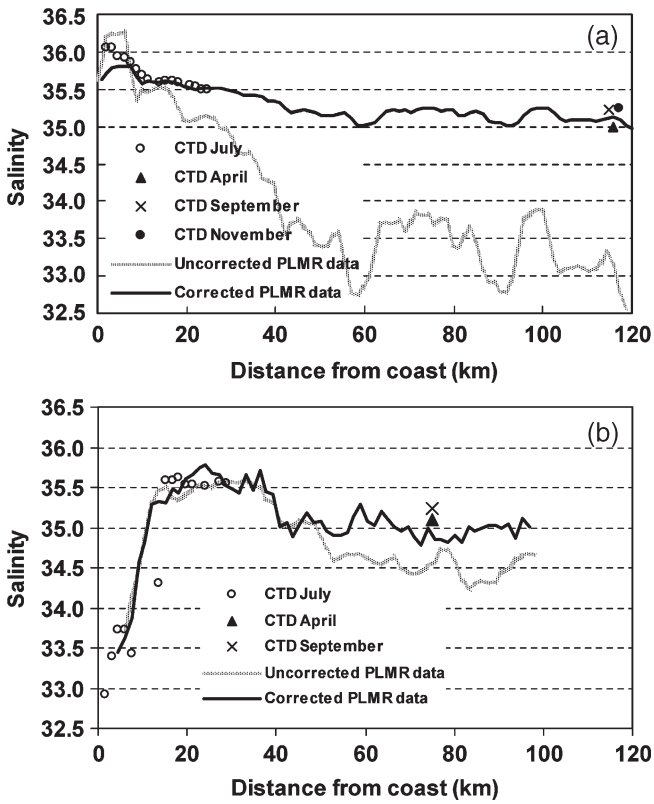

Fig. 5. Uncorrected and corrected PLMR data and CTD data on the (a) Townsville transect and (b) Lucinda transect. The CTD data that were taken in the inshore 30 km of the transects were used for correcting the PLMR data over the whole transects. The triangle and cross represent the data points of CTD salinity that were not used in the CTD–PLMR data correction process but were used for evaluation.

gaps in the PLMR data and very small changes in the salinity along the transects.

Fig. 5 shows the uncorrected and corrected PLMR and CTD data on the Townsville transect [Fig. 5(a)] and the Lucinda transect [Fig. 5(b)]. The CTD data in the inshore 30 km of the transects were used for correcting the PLMR data over the whole transects. Fig. 5 also shows the offshore data points of CTD salinity that are not used in the CTD–PLMR data correction process. It is notable that the corrected data show a significant improvement over the uncorrected data, confirming that the PLMR calibration needs careful attention. Before CTD data correction, the PLMR data are about 2 and 0.7 psu too low for the Townsville and Lucinda transects, respectively. After laboratory, the field data correction PLMR data are within 0.15 and 0.4 psu of the CTD data for Townsville and Lucinda, respectively. It should be noted that some of the discrepancy between the offshore PLMR and CTD data may be because the CTD data were not taken at the same time as the PLMR data. However, previous work has shown that the salinity of the western Coral Sea and the East Australian Current, which control the properties of the water outside the GBR off the continental shelf, is relatively constant [17], [18], [21].

Fig. 6 shows the differences between the PLMR and CTD data in all eight transects in the inshore 30 km before [Fig. 6(a)] and after [Fig. 6(b)] calibration using the CTD data. Before correction using the CTD data, when we use the PLMR data

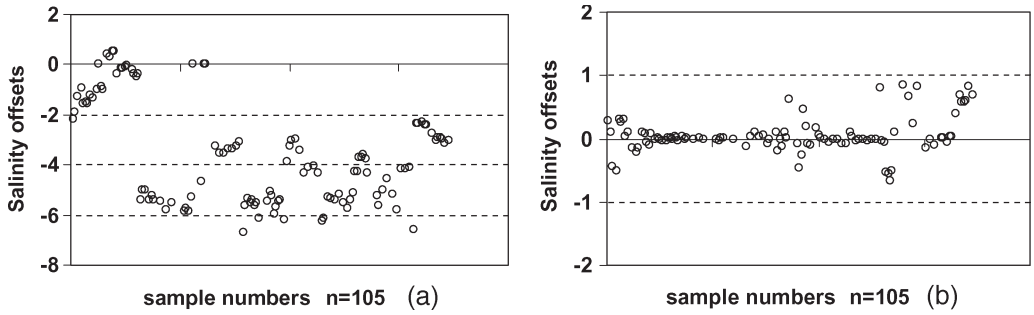

Fig. 6. Improvement in PLMR salinity estimates that were obtained by calibrating using *in situ* CTD measurements (a) before calibration and (b) after calibration. The sample numbers express all the values that were obtained from fieldwork and can also be compared between the PLMR and CTD data. The salinity offsets equal the PLMR values minus the CTD values. The positive values show that the PLMR data are higher than the CTD data, and the negative values show that the PLMR data are lower than the CTD data.

minus the CTD data, the mean offset is about −3.4 psu, and the variation for most values is about −3 to −6 psu [Fig. 6(a)]. After calibration using the CTD data, the mean of the difference between the PLMR and CTD salinities is about 0.16 psu, with a deviation of about 0 to ±0.5 psu [Fig. 6(b)].

B. Salinity Gradients in the GBR Lagoon

There is a considerable difference in the salinity gradients between the north and south of Townsville in the study area due to the freshwater input to the lagoon. To the north of Townsville (latitude 19.3° S), the southeasterly trade winds bring orographic rainfall for most of the year, and the coast is characterized by tropical rainforest and permanently flowing streams and creeks. At Townsville and to the south, the coast is characterized by Savannah grasslands and rivers with strong seasonal variation from dry beds in winter to floods in the wet season. It is instructive to plot (Fig. 7) the average cross-shelf salinity of all the southern transects (i.e., Bowen, Townsville, and Balgal) together with the average cross-shelf salinity of the northern transects (i.e., Lucinda and Russell) in the inshore 20 km during the winter (dry season) conditions. A clear difference between the northern average and southern average is seen within 20 km of the coast, indicating the influence of river discharge in the northern area; that is, the average salinity at the coast is about 0.4 psu higher in the south region and about 2 psu lower in the north region when compared with the nearly constant value 100 km offshore. It is also notable that a higher salinity exists at about 5 km from the shore in the northern transects from both the CTD and PLMR data and may be caused by hypersaline water moving northward from the drier southern region. At about 20 km offshore, the north–south differentiation disappears, and all transects tend to follow a decreasing salinity gradient of about 0.3 psu per 100 km from the 20-km point to the edge of the continental shelf.

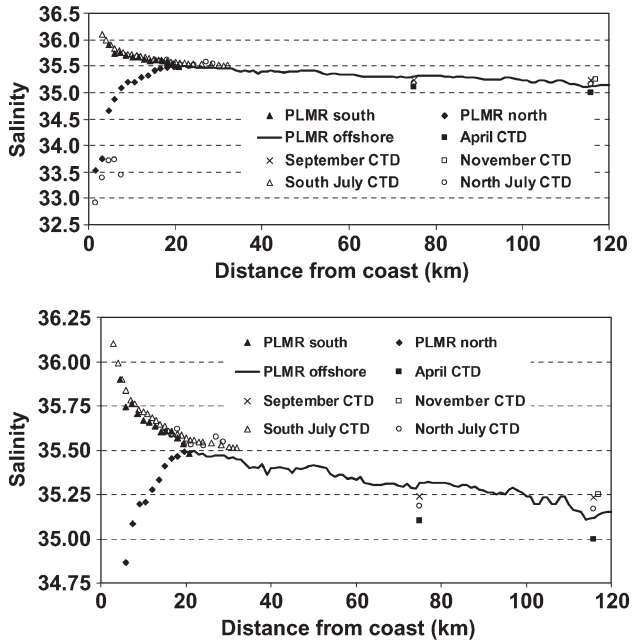

Fig. 7. Salinity gradient across shelf in the central GBR lagoon. PLMR south represents the average of the PLMR transects from Bowen, Townsville, and Balgal for the inshore 20 km. PLMR north represents the average of the PLMR transect from Lucinda and Russell in the inshore 20 km. PLMR offshore represents the average of the PLMR transect from all five transects from both northern and southern regions out to about 100 km from the shore. The lower panel is an expanded view of the upper panel.

IV. Discussion and Conclusion

The accuracy of the PLMR depends critically on the temperature regulation inside the instrument to provide a spatially and temporally uniform temperature distribution. It was found that a less than ideal temperature regulation was achieved with the middle of the antenna array being consistently 6 °C to 12 °C hotter than the other parts of the instrument. In addition, the temperature differentials changed with time by up to 5 °C along the transect (about 1-h duration). Problems maintaining a stable and uniform temperature caused considerable difficulties with the instrument calibration and required a modification of the calibration equation to improve the quality of the data. As a result of these field tests, a future program will develop hardware enhancements to increase insulation and investigate the provision of more heating power from the airplane.

The PLMR results that were obtained using the factory calibration, averaged over all beams and polarizations along a 1-km length of transect, were up to 3–6 psu (average 3.5 psu) lower than the measurements made with a CTD profiler but showed a high correlation with the CTD data. This high correlation allowed the use of the CTD data to correct the PLMR data for internal temperature effects and environmental effects. Some of the offset may be due to inadequacies in the correction for sea surface roughness due to the wind. Also, the reflected

radiation from the sky may be different on different days. In this analysis, we have assumed that the environmental effects remain constant for the duration and spatial extent of each transect. In this paper, the CTD data from the inshore 30 km of the transects were used to produce regression equations to correct the PLMR data. The corrected PLMR data were then tested against the other CTD measurements that were made in the offshore parts of the transects. It was found that the corrected PLMR measurements had an accuracy of between 0.1 and 0.8 psu (average 0.16 psu).

The combination of the CTD and PLMR data that were used in this paper enabled us to detect a significant difference in nearshore salinity gradients between areas adjacent to the dry and wet coastlines. The coast north of Townsville is adjacent to the rainforest-clad wet tropics districts, where some freshwater discharge to the coast exists through most of the year. In contrast, the area south of Townsville is usually very dry from May to December, and thus, there is usually no freshwater discharge to the coast. The data show that the southern part of the study area has a well-developed hypersaline coastal region with salinities reaching almost 1 psu above the waters of the Coral Sea. At the same time, the transects in the wet tropics region show nearshore water about 2 psu below the Coral Sea values. This may be caused by the local runoff in the wet tropics or by the alongshore movement of coastal water.

These initial tests of the PLMR instrument have shown that, despite the problems with internal temperature stability, a high degree of accuracy of salinity measurements can be achieved if small amounts of *in situ* CTD data are also collected. It should be noted that many of the temperature stability problems have been a result of a considerable reduction in the heater capacity over other instruments such as the SLFMR. The PLMR has a maximum heating capacity of 150 W, as compared with a value of 1 kW for the SLFMR. This reduction was necessary to fly from the smaller aircraft, which has a more limited power generation capacity. It is likely that considerable improvements to the PLMR will be made by using more thermal insulation within the instrument and a modest increase in the heating capacity. It is thus likely that a significant improvement in the PLMR performance is achievable following these initial tests.

ACKNOWLEDGMENT

The authors would like to thank M. Depczynski, C. Fulton, and J. Whinney for help with the collection of the *in situ* salinity data.

REFERENCES

[1] A. Camps, J. Font, C. Gabarro, N. Duffo, F. Torres, S. Blanch, A. Aguasca, R. Villarino, L. Enrique, J. J. Miranda, J. J. Arenas, A. Julia, J. Etcheto, V. Caselles, A. Weill, J. Boutin, S. Contardo, R. Niclos, R. Rivas, S. C. Reising, P. Wursteisen, M. Berger, and M. Martin-Neira, "The WISE 2000 and 2001 field experiments in support of the SMOS mission: Sea surface L-band brightness temperature observations and their application to sea surface salinity retrieval," *IEEE Trans. Geosci. Remote Sens.*, vol. 42, no. 4, pp. 804–823, Apr. 2004.

[2] H. J. C. Blume, B. M. Kendall, and J. C. Fedors, "Measurement of ocean temperature and salinity via microwave radiometry," *Boundary-Layer Meteorol.*, vol. 13, no. 1–4, pp. 295–308, Jan. 1978.

[3] D. M. Burrage, M. L. Heron, J. M. Hacker, J. L. Miller, T. C. Stieglitz, C. R. Steinberg, and A. Prytz, "Structure and influence of tropical river plumes in the Great Barrier Reef: Application and performance of an airborne sea surface salinity mapping system," *Remote Sens. Environ.*, vol. 85, no. 2, pp. 204–220, May 2003.

[4] D. M. Burrage, E. Campos, C. Martinez, T. Pérez, A. Piola, and J. Wesson, "An airborne salinity survey of the La Plata river plume," in *Proc. Aquarius/SAC-D-SMOS-HYDROS Joint Sci. and Implementation Workshop*, Miami, FL, Apr. 20–22, 2004. [Online]. Available: http://glaucus.fcien.edu.uy/pcmya/sacc/saccdocs/Burrage01/index.html

[5] M. A. Goodberlet, C. T. Swift, K. P. Kevin, J. L. Miller, and J. B. Zaitzeff, "Microwave remote sensing of coastal zone salinity," *J. Coast. Res.*, vol. 13, no. 2, pp. 363–372, 1997.

[6] M. A. Goodberlet and C. T. Swift, "A remote sensing system for measuring estuarine and coastal ocean surface salinity," Quadrant Eng., Hadley, MA, Progress Rep. 2, 1993.

[7] J. P. Hach, "A very sensitive airborne microwave radiometer using two reference temperatures," *IEEE Trans. Microw. Theory Tech.*, vol. MTT-16, no. 9, pp. 629–636, Sep. 1968.

[8] L. A. Klein and C. T. Swift, "An improved model for the dielectric constant of sea water at microwave frequencies," *IEEE Trans. Antennas Propag.*, vol. AP-25, no. 1, pp. 104–111, Jan. 1977.

[9] D. M. Le Vine, A. J. Griffis, C. T. Swift, and T. J. Jackson, "ESTAR: A synthetic aperture microwave radiometer for remote sensing applications," *Proc. IEEE*, vol. 82, no. 12, pp. 1787–1801, Dec. 1994.

[10] D. M. Le Vine, S. Abraham, Y. H. Kerr, W. J. Wilson, N. Skou, and S. S. Sobjaerg, "Comparison of model prediction with measurements of galactic background noise at L-band," *IEEE Trans. Geosci. Remote Sens.*, vol. 43, no. 9, pp. 2018–2023, Sep. 2005.

[11] J. L. Miller, "Airborne remote sensing of salinity," *Backscatter*, vol. 11, no. 3, pp. 24–27, 2000.

[12] J. L. Miller, *Salinity, Temperature and Roughness Remote Scanner (STARRS)*, 2001. [Online]. Available: http://www.cesbio.ups-tlse.fr/data_all/SMOS_WS/LESTER/NRL3/sld007.htm

[13] J. L. Miller, M. A. Goodberlet, and J. B. Zaitzeff, "Remote sensing of salinity in the coastal zone," *EOS, Trans. Amer. Geophys. Union*, vol. 79, no. 14, pp. 173–177, Apr. 1998.

[14] N. Skou, *Microwave Radiometer Systems: Design and Analysis*. Norwood, MA: Artech House, 1989, pp. 1–162.

[15] I. Skolnik, *Radar Handbook*. New York: McGraw-Hill, 1970, ch. 11.

[16] F. T. Ulaby, R. K. Moore, and A. K. Fung, "Microwave remote sensing: Active and passive," in *Microwave Remote Sensing Fundamentals and Radiometry*, vol. 1. Reading, MA: Addison-Wesley, 1981, ch. 6.

[17] T. Walker, "Seasonal salinity variations in Cleveland Bay, Northern Queensland," *Aust. J. Mar. Freshw. Res.*, vol. 32, pp. 143–149, 1981.

[18] T. Walker, "Lack of evidence for evaporation-driven circulation in the Great Barrier Reef Lagoon," *Aust. J. Mar. Freshw. Res.*, vol. 33, pp. 717–722, 1982.

[19] W. J. Wilson, S. H. Yueh, S. J. Dinardo, S. Chazanoff, A. Kitiyakara, F. K. Li, and Y. Rahmat-Samii, "Passive active L- and S-band (PALS) microwave sensor for ocean salinity and soil moisture measurements," *IEEE Trans. Geosci. Remote Sens.*, vol. 39, no. 5, pp. 1039–1048, May 2001.

[20] W. J. Wilson, S. H. Yueh, S. J. Dinardo, and F. K. Li, "High-stability L-band radiometer measurements of saltwater," *IEEE Trans. Geosci. Remote Sens.*, vol. 42, no. 9, pp. 1829–1835, Sep. 2004.

[21] E. Wolanski and B. Ruddick, "Water circulation and shelf waves in the northern Great Barrier Reef Lagoon," *Aust. J. Mar. Freshw. Res.*, vol. 32, pp. 721–740, 1981.

Yonghong Wang received the S.B. and S.M. degrees from Ocean University of China, Qingdao, in 1991 and 1995, respectively, and the Ph.D. degree in physical geography from the State Key Laboratory of Estuarine and Coastal Research, Shanghai, China, in 2003.

From August 2005 to August 2006, she was a Visiting Scholar with the School of Mathematics, Physics, and IT, James Cook University, Townsville, Australia, where she joined the work on the evaluation of a dual-polarized Polarimetric L-band Multibeam Radiometer, a new airborne microwave remote sensing radiometer, by measuring the salinity gradients across the shelf of the Great Barrier Reef lagoon. Her current fields of interest include the research on estuarine and coastal hydrodynamic and geomorphology by using various methods, including remote sensing.

Malcolm L. Heron (SM'93) received the B.Sc. and M.Sc. degrees in physics and the Ph.D. degree in radio science from the University of Auckland, Auckland, New Zealand, in 1965, 1967, and 1971, respectively.

Since 1971, he has held various positions in teaching, research, and for a term, senior management at James Cook University, Townsville, Australia. He has recently been appointed the Director of the Australian Coastal Ocean Radar Network, which is a national project to install and operate HF radars around Australia. His interests are in the physics of remote sensing, with current emphasis on HF techniques and microwave remote sensing of salinity.

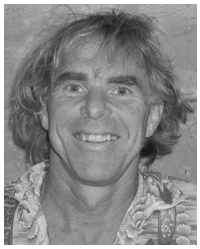

Arnstein Prytz received the B.Sc. (Hons.) degree from the Australian National University, Canberra, Australia, in 1981.

Since 1981, he has worked in various scientific capacities, mostly at James Cook University (JCU), Townsville, Australia, specializing in coastal ocean radar. He has been particularly involved with the data analysis from HF and VHF systems. In addition, he has worked with airborne radiometry, particularly for the detection of river flood plumes. He is currently with the Australian Coastal Ocean Radar Network, JCU, installing and maintaining a system of ocean radars for the continuous monitoring of some of Australia's coastline.

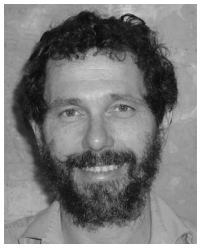

Peter V. Ridd received the Ph.D. degree from James Cook University (JCU), Townsville, Australia, in 1988, with a dissertation on antenna modeling for geophysical prospecting applications.

He is currently a Reader with the School of Mathematics, Physics, and IT, JCU. From 1984 to 1988 and, again, in 1991, he was an Oceanographer with the Australian Institute of Marine Science, Townsville. Since 1992, he has been with JCU, working primarily on coastal oceanography and instrument development. His primary interests are related to mangrove swamp hydrodynamics, sediment transport near coral reefs, and anthropogenic impacts on the Great Barrier Reef. He has developed several instruments for measuring water turbidity and deposition in natural environments.

Craig R. Steinberg received the B.Sc. degree (with honors) in meteorology and oceanography from the Flinders University of South Australia, Adelaide, in 1984.

In 1987, he joined the Australian Institute of Marine Science (AIMS), Townsville, Australia, as an Experimental Scientist. He undertakes physical oceanographic research in support of interdisciplinary studies with the Responding to Climate Change Research Team, AIMS. This involves observation, analysis, and numerical modeling on scales that range from individual reefs to the Coral Sea, of phenomena ranging from waves to ocean circulation. He is currently a Senior Experimental Scientist and joint Program Leader of the Coastal Processes and Modelling Program, AIMS@JCU. His current interests are impacts of tidal mixing on productivity hot spots, coral bleaching, and turbidity mapping. He also currently manages the remote sensing unit that provides extensive sea surface temperature and ocean color products for the public and the research community.

Jörg M. Hacker received the doctorate in atmospheric sciences (Dr. rer. nat.) from the University of Bonn, Bonn, Germany, in 1980.

Until 1982, he was a Research Fellow with the University of Bonn. In 1982, he was a Postdoctoral Fellow with the Flinders University of South Australia, Adelaide, where, from very small beginnings, he built up Australia's National Research Aircraft Facility, i.e., Airborne Research Australia (ARA), which today is Australia's only national facility that is engaged in using and operating aircraft for atmospheric and environmental research. He is currently the Director and Chief Scientist of ARA and an Associate Professor with the Flinders University of South Australia. He was instrumental in securing one of the very few civilian high-altitude research aircraft (the Grob G520T Egrett, which can fly research missions to altitudes as high as 15 km) for the facility and is now flying regularly as a Mission Specialist in this aircraft all over the world. His research work spans a wide area, with special emphasis on the atmospheric boundary layer and the development of innovative instrumentation and measurement strategies using airborne platforms. He is the coauthor of more than 50 papers published in internationally refereed journals and of more than 100 conference proceedings. He pioneered the concept of using cost-efficient small aircraft for atmospheric research, including the research described in this paper. He holds a pilot's license with several special endorsements and has more than 5000 flying hours in a wide range of aircraft, including flying gliders over the Andes in South America up to 12.5 km. In the context of his research, he regularly flies aircraft as low as 10 m above the ground.

Prof. Hacker, together with colleagues Prof. H. Kraus (University of Bonn) and Prof. P. Schwerdtfeger (Flinders University of South Australia), was a recipient of the prestigious Max Planck Prize from the German Alexander-von-Humboldt-Foundation and the Max-Planck-Society in 1994. In addition, together with H. W. Grosse, he holds the World Record for flying a self-launching glider over a 500-km triangle at an average speed of 172 km/h.